Mitochondrial transfer from bone marrow-derived stromal cells to pulmonary alveoli protects against acute lung injury

Mohammad Naimul Islam, **Shonit R. Das**, **Memet T. Emin**, **Michelle Wei**, **Li Sun**, **Kristin Westphalen**, **David J. Rowlands**, **Sadiqa K. Quadri**, **Sunita Bhattacharya**, and **Jahar Bhattacharya**[1]
Lung Biology Laboratory, Division of Pulmonary, Allergy & Critical Care Medicine, Department of Medicine, Columbia University, College of Physicians & Surgeons, New York, NY 10032, USA.

Abstract

Bone marrow-derived stromal cells (BMSCs) protect against acute lung injury (ALI). To determine the role of BMSC mitochondria in the protection, we airway-instilled mice first with lipopolysaccharide (LPS), then with mouse BMSCs (mBMSCs). Live optical studies revealed that mBMSCs formed connexin 43 (Cx43)-containing gap junctional channels (GJCs) with the alveolar epithelium, releasing mitochondria-containing microvesicles that the epithelium engulfed. The presence of BMSC mitochondria in the epithelium was evident optically, as also by the presence of human mitochondrial DNA in mouse lungs in which we instilled human BMSCs (hBMSCs). The mitochondrial transfer increased alveolar ATP. LPS-induced ALI, indicated by alveolar leukocytosis and protein leak, inhibition of surfactant secretion and high mortality, was markedly abrogated by wild type mBMSCs, but not by mutant, GJC-incompetent mBMSCs, or by mBMSCs with dysfunctional mitochondria. This is the first evidence that BMSCs protect against ALI by restituting alveolar bioenergetics through Cx43-dependent alveolar attachment and mitochondrial transfer.

Introduction

Exogenous administration of purified BMSCs protects in models of organ system injury[1–2], including sepsis-induced ALI[3–4], suggesting that BMSCs might be therapeutically effective[5]. However, the protective mechanisms are not entirely clear.

BMSCs might protect in sepsis-ALI by engrafting in the alveolar epithelium[6–7], although not all agree[8–9], or by paracrine secretions of keratinocyte growth factor (KGF)[10], interleukin-10 (IL-10)[11–12], angiopoietin-1[13–14], interleukin-1 receptor antagonist[15], and prostaglandin E2 (PGE2)[16].

Since sepsis-ALI impairs lung mitochondrial bioenergetics[17–19], we considered the possibility that the BMSC protective effect involves mitochondrial transfer to host cells. In culture, BMSCs transfer mitochondria to endothelial cells, A549 cells and

cardiomyocytes[20–22]. However in the BMSC-exposed intact lung, the extent of mitochondrial transfer and its potential therapeutic effect is not known. Here, we addressed these issues through live lung microscopy[23–24].

Results

mBMSCs attach to alveoli by forming Cx43-based GJCs

To establish the sepsis-ALI model, we airway instilled *E. coli* LPS in anesthetized mice. For control, we similarly instilled phosphate-buffered saline (PBS). After 4 h, we isolated and blood-perfused the lungs of the mice, then viewed the lungs by confocal or two-photon microscopy for a further 4 h[23–24]. To delineate alveoli, we loaded the alveolar epithelium with a water-soluble, cytosolic dye[23–24]. To fluorescently label mBMSCs, we expressed the mitochondria-targeted fluorescent protein, DsRed and confirmed that the expression was mitochondria localized (Supplementary Fig. 1a). Minutes after airway instillation, we detected DsRed-expressing mBMSCs adjacent to the alveolar epithelium (Fig. 1a).

In PBS lungs, instilled mBMSCs migrated from deep to superficial regions of the alveoli. Thus, when we viewed alveoli in 2 μm-thick optical sections at a fixed focal plane, we detected mBMSCs that emerged from deeper planes and progressively occupied epithelial sites at which no mBMSCs were previously present (Fig. 1a). Accordingly, DsRed fluorescence increased in a time dependent manner at sites of mBMSC emergence (Fig. 1b). In lungs that we isolated and imaged 24 h after airway instillations of PBS and mBMSCs, we no longer detected mBMSCs in the imaged alveoli (Fig. 1c), or in the lung as a whole (Fig. 1d), although they were present in the adjoining subpleural interstitium (Fig. 1c) and in thoracic lymph nodes (Fig. 1e).

In contrast to PBS lungs, in LPS lungs mBMSCs migrated less (Fig. 1b), the subpleural interstitium contained fewer mBMSCs and alveoli retained the cells to a greater extent (Fig. 1c). In addition, by flow cytometry we detected larger numbers of retained mBMSCs in the lung as a whole (Fig. 1d **and** Supplementary Fig. 1b). When we airway instilled mBMSCs containing a water-soluble dye of fluorescence different from that of the epithelial dye, within 30 minutes of instillation several alveolus-attached mBMSCs spontaneously exchanged cytosolic fluorescence with the alveolar epithelium (Fig. 1f). Since the dyes were membrane impermeable, the intercellular dye exchange suggested the presence of GJCs. To test this possibility, we quantified fluorescence recovery after photobleaching (FRAP)[20], which assays GJC-dependent communication. During photobleaching we imaged multiple optical sections in the cell's depth axis to confirm that mBMSC fluorescence was lost throughout the cell, thereby ruling out the possibility that the fluorescence recovery was due to intracellular dye diffusion. FRAP was present in alveolus-attached mBMSCs (Fig. 1f), confirming the presence of GJCs between the attached cells. Direct intra-alveolar microinfusions of the non-specific GJC blocker, α-glycyrrhetinic acid, or the specific Cx43-inhibiting peptide, GAP26[23,25], each blocked the FRAP (Fig. 1g), implicating Cx43 in the GJC formation.

Under culture conditions, mBMSCs that express Cx43 with T→A mutation at threonine 154 (mutCx43) do not form functional GJCs[20,26]. mBMSCs expressing mutCx43 markedly decreased endogenous Cx43 (Supplementary Fig. 1c), indicating that the mutant negatively regulated Cx43 expression. When we instilled mutCx43-expressing mBMSCs in LPS lungs, the mutant mBMSCs migrated out of the lungs at rates similar to that of wild-type mBMSCs in PBS lungs (Fig. 1d, e). The mutant mBMSCs did not develop spontaneous dye exchange (not shown) or FRAP (Fig. 1g), indicating that wild-type Cx43 expression in mBMSCs was essential for the GJC formation and alveolar attachment. Spontaneous dye transfer and

FRAP were also absent under control conditions (instillation of PBS instead of LPS, or of 3T3 cells instead of mBMSCs) (not shown).

Within 4 h after airway instillation of LPS alone, that is in the absence of instilled mBMSCs or other cells, Cx43 fluorescence of the alveolar epithelium increased markedly (Fig. 2a), indicating that LPS alone induced a Cx43-rich alveolar membrane prior to the alveolar arrival of mBMSCs. Line-scan fluorescence analyses in LPS lungs revealed that the distribution of Cx43 in the alveolar epithelium was spatially uneven and that mBMSC attachment occurred at sites of high Cx43 expression (Fig. 2b). In primary isolates of AT2 cells[27] and lung membrane fractions that we recovered 4 h after airway instillation, mRNA analyses and immunoblots indicated that Cx43 expression was higher in LPS than in PBS lungs (Fig. 2c). However after 24 h, the expressions were similar between the groups (Fig. 2c). In isolated AT2 cells and in a non-characterized mixture of lung cells, mRNA analyses for known alveolar connexins[23] revealed that mBMSCs expressed only Cx43, and that this was the only connexin common to the lung cells and the mBMSCs (Fig. 2d), implicating Cx43 as the essential connexin in the present GJC formation. Since 3T3 cells also express Cx43[28], but did not form GJCs in LPS lungs (see above), we considered the effects of cell suspension, a condition to which we exposed the cells for ~2 h prior to airway instillation. Cx43 expressions were similar in plated mBMSCs and 3T3 cells. However, after we suspended the cells for 2 h in medium, the expression was lower by 44% in 3T3 cells than in mBMSCs (Supplementary Fig. 2a).

Alveolus-attached mBMSCs form nanotubes and microvesicles

Within 4 h after instillation of DsRed-expressing mBMSCs, approximately half of the alveolus-attached mBMSCs generated microvesicles and nanotubes (Fig. 3a, b). Released microvesicles were DsRed positive and they moved away from the cell body at a rate (1.8 ± 0.5 μm min^{-1}) similar to the flow of alveolar wall liquid[24] (Fig. 3a), suggesting that the microvesicles contained mitochondria and that they were convectively transported. Wild-type mBMSCs when plated in culture replicated similar behavior in that they spontaneously formed mitochondriatransporting nanotubes (Supplementary Fig. 2b). Plated mBMSCs inter-communicated induced Ca^{2+} increases, an effect that was not present in mBMSCs expressing mutCx43 (Supplementary Fig. 2c), suggesting that the Ca^{2+} communication was GJC dependent. Although mutCx43-expressing mBMSCs also formed nanotubes in culture (not shown), they did not support Ca^{2+} communication (Supplementary Fig. 2c). Moreover, they failed to form nanotubes or microvesicles when airway-instilled in LPS lungs (Fig. 3b), presumably because they failed to attach to alveoli (Fig. 1d, g). Nanotubes and microvesicles also failed to form in wild-type mBMSCs that we instilled in PBS lungs, or in 3T3 cells that we instilled in LPS lungs (not shown). Microvesicle budding was not present in a subset of wild-type mBMSCs that failed to form GJCs in LPS lungs, indicating that mBMSC attachment to the alveolar epithelium was essential for the effect. Flow cytometry determinations in supernatants of LPS lungs indicated that mBMSC microvesicle formation was extensive in the lung as a whole (Fig. 3c), increasing in 4 h but decreasing 20 h after mBMSC instillation (Fig. 3c, Supplementary Fig. 2d).

To gain mechanistic insights in nanotube formation[22,29], we airway instilled mBMSCs containing a cytosolic Ca^{2+} indicator. In LPS lungs, alveolar attachment caused time dependent Ca^{2+} increases in mBMSCs (Fig. 3d-f). Since alveolar treatment with GAP26 blocked the effect (Fig. 3f), we interpret that the Ca^{2+} increase was GJC dependent. When we instilled LPS lungs with mBMSCs that we previously loaded with a Ca^{2+} chelator, the mBMSCs successfully attached to the alveolar wall, but they failed to increase Ca^{2+} or to form nanotubes and microvesicles (Supplementary Fig. 2d), suggesting that these structural responses resulted from gap junctional Ca^{2+} communication.

mBMSCs transfer mitochondria to the alveolar epithelium

Mitochondrial transfer was evident in that alveolus-attached mBMSCs lost DsRed fluorescence, while the adjoining epithelium internalized the fluorescence. When we imaged the alveolar epithelium at different optical sections, the epithelial internalization of mBMSC mitochondria was evident in the merger of the DsRed and calcein colors, which resulted in intermediate pseudocolors in the epithelial cytosol (Fig. 3g). Trypan Blue, a cell-impermeable fluorescence quencher that decreases extracellular fluorescence[30], failed to decrease the internalized DsRed fluorescence (not shown), affirming the internalization. Following the mitochondrial transfer, mBMSC cell bodies lacking DsRed-labeled mitochondria remained attached to the apical alveolar epithelium (Fig. 3g), but did not intercalate in the alveolar wall.

The possibility that mBMSC microvesicles were engulfed by the epithelium was indicated in that the dynamin inhibitor[31], Dynasore, blocked mitochondrial transfer (Fig. 3h), implicating endocytosis in the engulfment mechanism. In support of this possibility, DsRed-positive microvesicles, that we recovered from LPS lungs in which we previously instilled wild-type mBMSCs, stained positively for Cx43 (Supplementary Fig. 2e). Further, instillation of mutCx43-expressing mBMSCs markedly decreased our recovery of microvesicles from LPS lungs (Fig. 3b).

Internalization of DsRed-expressing mBMSC mitochondria was best evident in AT2 cells 24 h after the instillations of LPS and mitochondrial DsRed-expressing mBMSCs. Although we did not confirm the internalization in alveolar type 1 cells, to determine the effect in AT2 cells, we loaded alveoli with fluorescent surfactant protein B (SPB) that localizes to lamellar bodies (LBs) that are present only in AT2 cells (Fig. 4a). Then we imaged single AT2 cells by confocal microscopy in a series of 1 μm-thick optical sections along the depth axis from the plane of the alveolar lumen towards the pleural plane. During this serial imaging, the images transitioned from dark signals at the air-filled plane to fluorescent signals on the cytosolic aspect of the air-epithelium border. mBMSC mitochondria were evident as DsRed-containing particles that interspersed with perinuclear LB clusters (Fig. 4b), affirming intracellular localization of the acquired mitochondria in AT2 cells.

To further validate the mitochondrial transfer, we instilled human BMSCs (hBMSCs) in PBS- or LPS-treated mice. Then 24 h later, we isolated AT2 cells and a mixed population of lung cells (Supplementary Fig. 3a-f), in which we PCR-amplified DNA sequences for human cytochrome oxidases 1 and 2 (*hCO1* and *hCO2*) (Fig. 4c **and** Supplementary Fig. 3g), which are transcribed by mitochondrial DNA. The presence of these human DNA sequences in mouse AT2 cells derived from LPS, but not PBS lungs further affirms that following LPS-induced lung injury, AT2 cells acquired mitochondria from the instilled hBMSCs. In support, flow cytometry of primary isolates of lung cells indicated that DsRed- and SPB-positive cells co-localized in the same cell cluster, consistent with the interpretation that the mBMSC mitochondria were located in AT2 cells (Fig. 4d **and** Supplementary Fig. 3h, i). No mitochondrial transfer was evident after instillation of mutCx43 -expressing mBMSCs (Fig. 4d).

mBMSC mitochondria increase alveolar ATP

We confirmed that ATP was lower in LPS than in PBS lungs[32–33]. We showed further that after we instilled wild type mBMSCs, lung ATP was similar for the two groups (Fig. 5a). Major ATP production in lung occurs through mitochondrial electron transport, which is inhibited by siRNA knockdown of the Rieske iron-sulfur protein (RISP) of complex III[30,34]. Expression of anti-RISP siRNA (siRISP), but not scrambled siRNA (scRISP) decreased

RISP expression and ATP in mBMSCs (Supplementary Fig. 4a, b), affirming the role of RISP in the ATP production.

siRISP expression did not adversely affect mBMSCs to the extent that the cells showed no evidence of apoptosis (Supplementary Fig. 4c) and their mitochondrial protein content was not different from wild type (not shown). The siRISP-expressing mBMSCs were functionally competent in that they formed alveolar attachments (not shown) and transferred mitochondria to AT2 cells (Supplementary Fig. 3i). However, both siRISP- and mutCx43-expressing mBMSCs failed to rescue ATP production in LPS lungs (Fig. 5a).

The availability of the fluorescent ATP probe, GlnKII-GFP (Perceval)[35] enabled direct determinations of single-cell ATP in live alveoli. We confirmed expression of the probe in the lung by immunoblotting (Supplementary Fig. 5a). Both immunofluorescence and GFP fluorescence of the probe was widely expressed in the alveolar epithelium in all regions of the lung's surface (Fig. 5b). We confirmed that the expressed ATP fluorescence was appropriately responsive to cell ATP, which we altered by glucose depletion and replenishment in the lung perfusate (Supplementary Fig. 5b)[35].

In lungs that we imaged 24 h after instillation, alveolar ATP fluorescence was lower in LPS than PBS lungs (Fig. 5b). However in both groups of lungs the fluorescence was similar after we instilled wild type, but not mutCx43-expressing mBMSCs (Fig. 5b, c). Mitochondrial transfer to a localized alveolar segment increased ATP fluorescence not only throughout the same alveolus, but also in 8–10 adjacent alveoli (Fig. 5d). Within 5–8 h of instilling mBMSCs, time-lapse imaging indicated that the increase of ATP fluorescence spread progressively from the site of mitochondrial transfer to other sites in the alveolar wall (Fig. 5e). In the absence of mBMSC instillation, time-lapse ATP fluorescence tended to decrease, although this change was not statistically significant (Fig.5f).

mBMSC mitochondria protect against ALI

To assay an ATP-dependent alveolar functional response, we quantified surfactant secretion from AT2 cells of intact alveoli as the rate of LB exocytosis responsive to a brief lung expansion[36]. We could not induce the secretion in LPS lungs, except after we instilled wild-type mBMSCs (Figs. 6a, b), but not mBMSCs expressing siRISP or mutCx43 (Figs. 6a, b).

Globally, LPS induced the expected ALI responses, namely increased leukocytosis in the bronchoalveolar lavage (BAL) (Fig. 6c), increased albumin leakage in the BAL (Supplementary Fig. 6), and decreased mouse survival (Fig. 6d). In confirmation of previous reports[11,16], wild type mBMSCs markedly abrogated these responses. Our new findings are that mBMSCs expressing siRISP, siRNA against Cx43, or mutCx43 did not ameliorate the BAL leukocytosis or the mouse survival (Fig. 6c, d).

Discussion

Our findings indicate that alveolar attachment, hence lung retention of the migration-prone BMSCs was critical for the ensuing protective effects against ALI. Following alveolar attachment, BMSCs transferred mitochondria to the alveolar epithelium, an event that occurred progressively for 24 h, accounting for the protective effect. BMSCs carrying defective mitochondria failed to protect. Cx43 was the critical mechanism underlying alveolar attachment of wild-type BMSCs that generated Cx43-expressing nanotubes and microvesicles in a Ca^{2+} dependent manner. Epithelial engulfment of the released microvesicles might have contributed to the mitochondrial transfer. Microvesicles formed extensively in the lung and their parenchymal dispersal might have been convective[24,37].

Together, these findings provide the first *in vivo* evidence that BMSCs establish epithelial interactions, form microstructures and transfer mitochondria to host cells.

The mitochondrial transfer increased alveolar ATP in LPS lungs in a Cx43-dependent manner. Single-cell ATP determinations, the first in an intact organ, indicated that the ATP increase occurred at the transfer site as well as in adjoining alveoli, affirming that the transferred mitochondria were live and capable of ATP generation in the recipient epithelium. Inflation-induced alveolar surfactant secretion, a major ATP-dependent process that regulates alveolar stability[38–39], provides a functional metric of alveolar bioenergetics. The fact that we could induce the secretion in LPS lungs only after instillation of wild-type BMSCs, but not of BMSCs carrying dysfunctional mitochondria, underlines the importance of bioenergetics restoration in cell repair therapy.

We confirmed that BMSCs increased mouse survival in LPS-ALI[11], and we showed further that the survival advantage was lost if the BMSCs contained dysfunctional mitochondria or GJCincompetent Cx43, or if they were depleted of Cx43. These findings further support Cx43-dependent mechanisms and transfer of viable mitochondria in the protective response. Although long-term consequences of mitochondrial transfer need to be understood, evidently the transfer was sufficiently rapid to be protective in the acute phase of lung injury.

Unanswered questions include the relative roles of paracrine secretion[11–12,16] versus mitochondrial transfer in the BMSC protective effect. Although mitochondrial loss in alveolus-attached BMSCs could decrease ATP in these cells, thereby decreasing their secretory capacity, protective paracrine secretions could continue from non-attached, mitochondria-competent BMSCs. The combined effects of these different sets of BMSCs require clarification. Also unclear is how increase of alveolar ATP repairs the alveolar epithelial and endothelial barriers that are pathologically defective in ALI. Although these issues require attention, we propose that exogenous BMSCs provide a "Trojan horse" therapeutic strategy for supplying fresh mitochondria to injured cells, thereby enhancing cellular bioenergetics and improving organ function in ALI and other inflammatory diseases.

Methods

Cells

The Institutional Animal Care and Use Committee of Columbia University Medical Center approved all animal procedures. We harvested, cultured and characterized mBMSCs from male C57BL/6J mice (The Jackson Laboratory) as we previously reported[20,40]. Briefly, in anesthetized mice (ketamine 100 mg kg^{-1} and xylazine 5 mg kg^{-1} i.p.), we infused MSC growth medium in femurs and tibia lumens to recover marrow. We plated the marrow in tissue culture flasks. After 3 d, we rejected the supernatant and cultured adherent mBMSCs (37 °C) and used them after 5–15 passages. Subsequently, we transfected the mBMSCs with plasmids for mutCx43 or mitochondrial DsRed[20]. To knockdown RISP or Cx43, we incubated the mBMSCs for 48 h with fluorophore (Dy547)-conjugated siRNA or scRNA constructs in complex with lipofectin[30,34]. To load the cytosol, we incubated mBMSCs with the water-soluble dye, calcein red (5 μM, 20 min). To stain the cell membrane, we incubated mBMSCs sequentially with biotin (0.5 μg μl^{-1}, 20 min) and Alexa 633-tagged streptavidin (0.5 μg μl^{-1}, 20 min). We obtained hBMSCs from the Institute of Regenerative Medicine, Texas A&M Health Science Center. We cultured hBMSCs in minimum essential medium (α-MEM), which we supplemented with 10% fetal bovine serum (FBS), 5% horse serum and 1% of an antibiotic mixture under 5% CO2 at 37 °C, and we used the cells after 3–5 passages. We purchased mouse fibroblasts (3T3 cells) and human embryonic kidney (HEK)

cells from ATCC and cultured them in 5% CO_2 at 37 °C in Dulbecco's modified eagle medium (DMEM) containing 10% FBS and 1% of an antibiotic mixture.

ALI

We gave LPS in sterile PBS (40 μl) by intranasal instillation to anesthetized mice. LPS concentration was 1 mg kg^{-1} for all experiments and 10 mg kg^{-1} for the survival experiments. For control, we instilled an equal volume of sterile PBS. For lung instillation of mBMSCs (2×10^5 cells in 40 μl PBS), 4 h after LPS or PBS, we intratracheally instilled the mBMSCs in isolated and blood-perfused lungs derived from the LPS- or PBS-treated mice, or we gave the mBMSCs by intranasal instillation to anesthetized mice from which we recovered the lungs after 24 h.

Imaging

We imaged isolated, blood-perfused lungs by confocal (LSM 510 META, Zeiss) or two-photon microscopy (Radiance 2100, Zeiss)[23–24]. Except where we state otherwise, we set the optical thickness at 2 and 0.6 μm for confocal and two-photon imaging, respectively. For FRAP determinations, we photobleached the cytosolic fluorescence of calcein in selected mBMSCs using high power laser excitation, then imaged fluorescence recovery at 1 frame min^{-1}. In all runs we obtained optical sections across the cell's vertical diameter to confirm that the photobleaching was complete throughout the cell. We analyzed the images using commercial software (MetaMorph 6.3, Universal Imaging).

mBMSC counts

To quantify alveolar mBMSCs by imaging, we counted the numbers of DsRed or Hoechst 33342 spots in a fixed imaging plane. To determine mBMSC numbers in the lung by flow cytometry (Supplementary Methods), we gave intranasal instillations of mBMSCs stained with fluorescence-conjugated streptavidin, then recovered lung cells (Supplementary Methods) after 24 h. To determine mBMSC numbers in lymph nodes, we isolated thoracic lymph nodes 24 h after PBS or LPS. We viewed the nodes by two-photon microscopy to count cells positive for Hoechst 33342 in 15 optical sections across a tissue depth of 50 μm.

ATP assay

For tissue determinations, we assayed tissue lysate using a commercially available kit (Abcam Inc.). For single cell determinations, we transfected alveoli with the probe, GlnK-GFP (Perceval, gift of Dr. G. Yelen, Harvard University)[35]. We complexed the Perceval plasmid (2.5 μg $μl^{-1}$) with liposomes (20 μg $μl^{-1}$, 100-nm pore size; DOTAP, Avanti Lipids) that we suspended in sterile PBS to a final plasmid concentration of 1 μg $μl^{-1}$. We gave mice intranasal instillations of the plasmid-liposome mixture (50 μl), then 48 h later we imaged Perceval fluorescence in alveoli. For control, we transfected empty vector.

Data analysis

We carried out paired comparisons by the paired t-test and multiple comparisons by ANOVA with Bonferroni's post-hoc analysis. All data are mean ± SE. We accepted significance at *$p < 0.05$*.

Supplementary Material

Refer to Web version on PubMed Central for supplementary material.

Acknowledgments

References

1. Prockop DJ, Kota DJ, Bazhanov N, Reger RL. Evolving paradigms for repair of tissues by adult stem/progenitor cells (MSCs). Journal of cellular and molecular medicine. 2010; 14:2190–2199. [PubMed: 20716123]

2. Parekkadan B, Milwid JM. Mesenchymal stem cells as therapeutics. Annu Rev Biomed Eng. 2010; 12:87–117. [PubMed: 20415588]

3. Weiss DJ, Kolls JK, Ortiz LA, Panoskaltsis-Mortari A, Prockop DJ. Stem cells and cell therapies in lung biology and lung diseases. Proceedings of the American Thoracic Society. 2008; 5:637–667. [PubMed: 18625757]

4. Matthay MA, Goolaerts A, Howard JP, Lee JW. Mesenchymal stem cells for acute lung injury: preclinical evidence. Critical care medicine. 2010; 38:S569–S573. [PubMed: 21164399]

5. Rubenfeld GD, et al. Incidence and outcomes of acute lung injury. The New England journal of medicine. 2005; 353:1685–1693. [PubMed: 16236739]

6. Krause DS, et al. Multi-organ, multi-lineage engraftment by a single bone marrowderived stem cell. Cell. 2001; 105:369–377. [PubMed: 11348593]

7. Ortiz LA, et al. Mesenchymal stem cell engraftment in lung is enhanced in response to bleomycin exposure and ameliorates its fibrotic effects. Proceedings of the National Academy of Sciences of the United States of America. 2003; 100:8407–8411. [PubMed: 12815096]

8. Chang JC, Summer R, Sun X, Fitzsimmons K, Fine A. Evidence that bone marrow cells do not contribute to the alveolar epithelium. American journal of respiratory cell and molecular biology. 2005; 33:335–342. [PubMed: 15961725]

9. Kotton DN, Fabian AJ, Mulligan RC. Failure of bone marrow to reconstitute lung epithelium. American journal of respiratory cell and molecular biology. 2005; 33:328–334. [PubMed: 15961722]

10. Lee JW, Fang X, Gupta N, Serikov V, Matthay MA. Allogeneic human mesenchymal stem cells for treatment of E. coli endotoxin-induced acute lung injury in the ex vivo perfused human lung. Proceedings of the National Academy of Sciences of the United States of America. 2009; 106:16357–16362. [PubMed: 19721001]

11. Gupta N, et al. Intrapulmonary delivery of bone marrow-derived mesenchymal stem cells improves survival and attenuates endotoxin-induced acute lung injury in mice. Journal of immunology. 2007; 179:1855–1863.

12. Curley GF, et al. Mesenchymal stem cells enhance recovery and repair following ventilator-induced lung injury in the rat. Thorax. 2011

13. Mei SH, et al. Prevention of LPS-induced acute lung injury in mice by mesenchymal stem cells overexpressing angiopoietin 1. PLoS medicine. 2007; 4:e269. [PubMed: 17803352]

14. Xu J, et al. Mesenchymal stem cell-based angiopoietin-1 gene therapy for acute lung injury induced by lipopolysaccharide in mice. The Journal of pathology. 2008; 214:472–481. [PubMed: 18213733]

15. Ortiz LA, et al. Interleukin 1 receptor antagonist mediates the antiinflammatory and antifibrotic effect of mesenchymal stem cells during lung injury. Proceedings of the National Academy of Sciences of the United States of America. 2007; 104:11002–11007. [PubMed: 17569781]

16. Nemeth K, et al. Bone marrow stromal cells attenuate sepsis via prostaglandin E(2)-dependent reprogramming of host macrophages to increase their interleukin-10 production. Nature medicine. 2009; 15:42–49.

17. Dada LA, Sznajder JI. Mitochondrial Ca2+ and ROS take center stage to orchestrate TNF-alpha-mediated inflammatory responses. The Journal of clinical investigation. 2011

18. Harrois A, Huet O, Duranteau J. Alterations of mitochondrial function in sepsis and critical illness. Curr Opin Anaesthesiol. 2009; 22:143–149. [PubMed: 19390243]

19. Brealey D, et al. Association between mitochondrial dysfunction and severity and outcome of septic shock. Lancet. 2002; 360:219–223. [PubMed: 12133657]

20. Otsu K, et al. Concentration-dependent inhibition of angiogenesis by mesenchymal stem cells. Blood. 2009; 113:4197–4205. [PubMed: 19036701]

21. Spees JL, Olson SD, Whitney MJ, Prockop DJ. Mitochondrial transfer between cells can rescue aerobic respiration. Proceedings of the National Academy of Sciences of the United States of America. 2006; 103:1283–1288. [PubMed: 16432190]

22. Plotnikov EY, et al. Cell-to-cell cross-talk between mesenchymal stem cells and cardiomyocytes in co-culture. Journal of cellular and molecular medicine. 2008; 12:1622–1631. [PubMed: 18088382]

23. Parthasarathi K, et al. Connexin 43 mediates spread of Ca2+-dependent proinflammatory responses in lung capillaries. The Journal of clinical investigation. 2006; 116:2193–2200. [PubMed: 16878174]

24. Lindert J, Perlman CE, Parthasarathi K, Bhattacharya J. Chloride-dependent secretion of alveolar wall liquid determined by optical-sectioning microscopy. American journal of respiratory cell and molecular biology. 2007; 36:688–696. [PubMed: 17290033]

25. Hawat G, Benderdour M, Rousseau G, Baroudi G. Connexin 43 mimetic peptide Gap26 confers protection to intact heart against myocardial ischemia injury. Pflugers Arch. 2010; 460:583–592. [PubMed: 20514543]

26. Beahm DL, et al. Mutation of a conserved threonine in the third transmembrane helix of alpha- and beta-connexins creates a dominant-negative closed gap junction channel. The Journal of biological chemistry. 2006; 281:7994–8009. [PubMed: 16407179]

27. Corti M, Brody AR, Harrison JH. Isolation and primary culture of murine alveolar type II cells. Am J Respir Cell Mol Biol. 1996; 14:309–315. [PubMed: 8600933]

28. Das Sarma J, et al. Multimeric connexin interactions prior to the trans-Golgi network. J Cell Sci. 2001; 114:4013–4024. [PubMed: 11739633]

29. Rustom A, Saffrich R, Markovic I, Walther P, Gerdes HH. Nanotubular highways for intercellular organelle transport. Science. 2004; 303:1007–1010. [PubMed: 14963329]

30. Rowlands DJ, et al. Activation of TNFR1 ectodomain shedding by mitochondrial Ca2+ determines the severity of inflammation in mouse lung microvessels. The Journal of clinical investigation. 2011; 121:1986–1999. [PubMed: 21519143]

31. Macia E, et al. Dynasore, a cell-permeable inhibitor of dynamin. Dev Cell. 2006; 10:839–850. [PubMed: 16740485]

32. Heller AR, et al. Adenosine A1 and A2 receptor agonists reduce endotoxin-induced cellular energy depletion and oedema formation in the lung. European journal of anaesthesiology. 2007; 24:258–266. [PubMed: 17094869]

33. Kao SJ, Liu DD, Su CF, Chen HI. Niacinamide abrogates the organ dysfunction and acute lung injury caused by endotoxin. J Cardiovasc Pharmacol. 2007; 50:333–342. [PubMed: 17878764]

34. Guzy RD, et al. Mitochondrial complex III is required for hypoxia-induced ROS production and cellular oxygen sensing. Cell metabolism. 2005; 1:401–408. [PubMed: 16054089]

35. Berg J, Hung YP, Yellen G. A genetically encoded fluorescent reporter of ATP:ADP ratio. Nature methods. 2009; 6:161–166. [PubMed: 19122669]

36. Ashino Y, Ying X, Dobbs LG, Bhattacharya J. [Ca(2+)](i) oscillations regulate type II cell exocytosis in the pulmonary alveolus. American journal of physiology. Lung cellular and molecular physiology. 2000; 279:L5–L13. [PubMed: 10893197]

37. Wang PM, Ashino Y, Ichimura H, Bhattacharya J. Rapid alveolar liquid removal by a novel convective mechanism. American journal of physiology. Lung cellular and molecular physiology. 2001; 281:L1327–L1334. [PubMed: 11704526]

38. Whitsett JA, Wert SE, Weaver TE. Alveolar surfactant homeostasis and the pathogenesis of pulmonary disease. Annu Rev Med. 2010; 61:105–119. [PubMed: 19824815]

39. Dietl P, Haller T. Exocytosis of lung surfactant: from the secretory vesicle to the air-liquid interface. Annu Rev Physiol. 2005; 67:595–621. [PubMed: 15709972]

40. Dominici M, et al. Minimal criteria for defining multipotent mesenchymal stromal cells. The International Society for Cellular Therapy position statement. Cytotherapy. 2006; 8:315–317. [PubMed: 16923606]
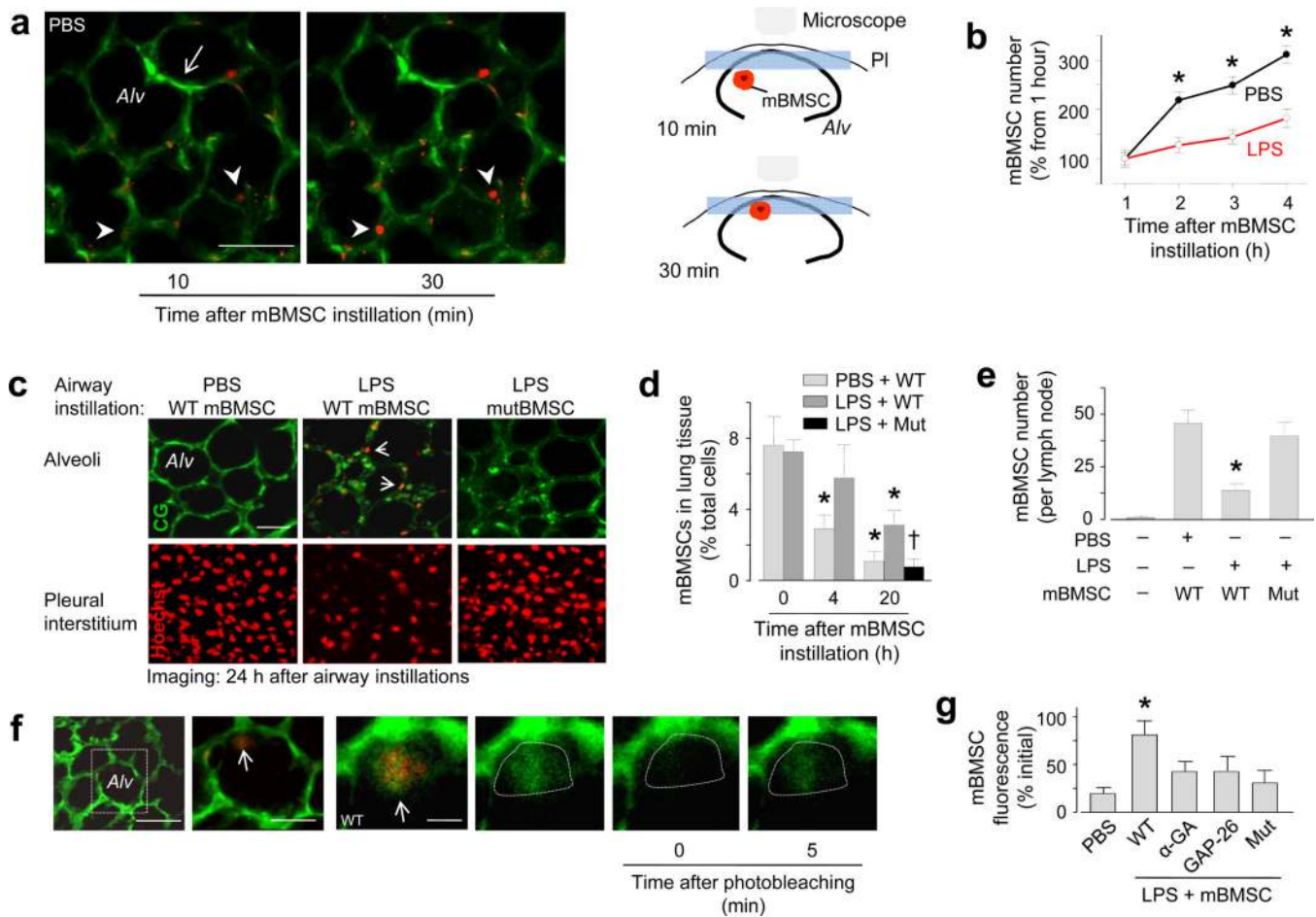
Figure 1. mBMSCs in live alveoli

Alv, alveolus. *Green,* calcein green. *Red, m*BMSCs with mitochondrial DsRed (*a, b*), Hoechst 33342 (*c*), fluorescence-tagged streptavidin (*e*), or calcein red (*f*). *Mut,* mBMSCs expressing mutant Cx43. (**a**) Images of mBMSCs (*arrowheads*) and alveolar septa (*arrow*). *Line,* 30 μm. Cartoons illustrate mBMSC migration to the imaged plane (*blue rectangle*). *Pl,* pleura. (**b**) Alveolar mBMSCs imaged at a fixed focal plane. Data are for 100 alveoli from 6 lungs for each group. * *p < 0.05* versus LPS. (**c**) Two-photon images (optical slice thickness 0.6 μm) at focal planes 4 (*top panel*) and 1 μm (*bottom panel)* deep to the visceral pleura. Replicated in 6 lungs for each group. *Line,* 30 μm. (**d**) Quantification of lung mBMSCs by flow cytometry. *n = 4* lungs for each bar; * *p < 0.05* versus 0 h, †*p < 0.05* versus bar on immediate left. (**e**) mBMSCs in thoracic lymph nodes. *n = 6* lymph nodes for each bar; * *p < 0.05* versus PBS. (**f**) Images show alveoli in an LPS lung (*first image*). *Line*, 20 μm. Magnification of the rectangle (*second image*) shows an mBMSC (*arrow*) in an alveolus. *Line*, 10 μm. Higher magnification (*third image*) shows green fluorescence in the mBMSC (*arrow*). Green channel renditions (*fourth to sixth image*) show responses to photobleaching in the area within the dotted line. *Line,* 3 μm. (**g**) Group data show FRAP responses in mBMSCs. *n = 15* cells each bar, * *p < 0.05* versus PBS. *α-GA*, α-glycyrrhetinic acid; *Gap26*, Cx43 inhibiting peptide.
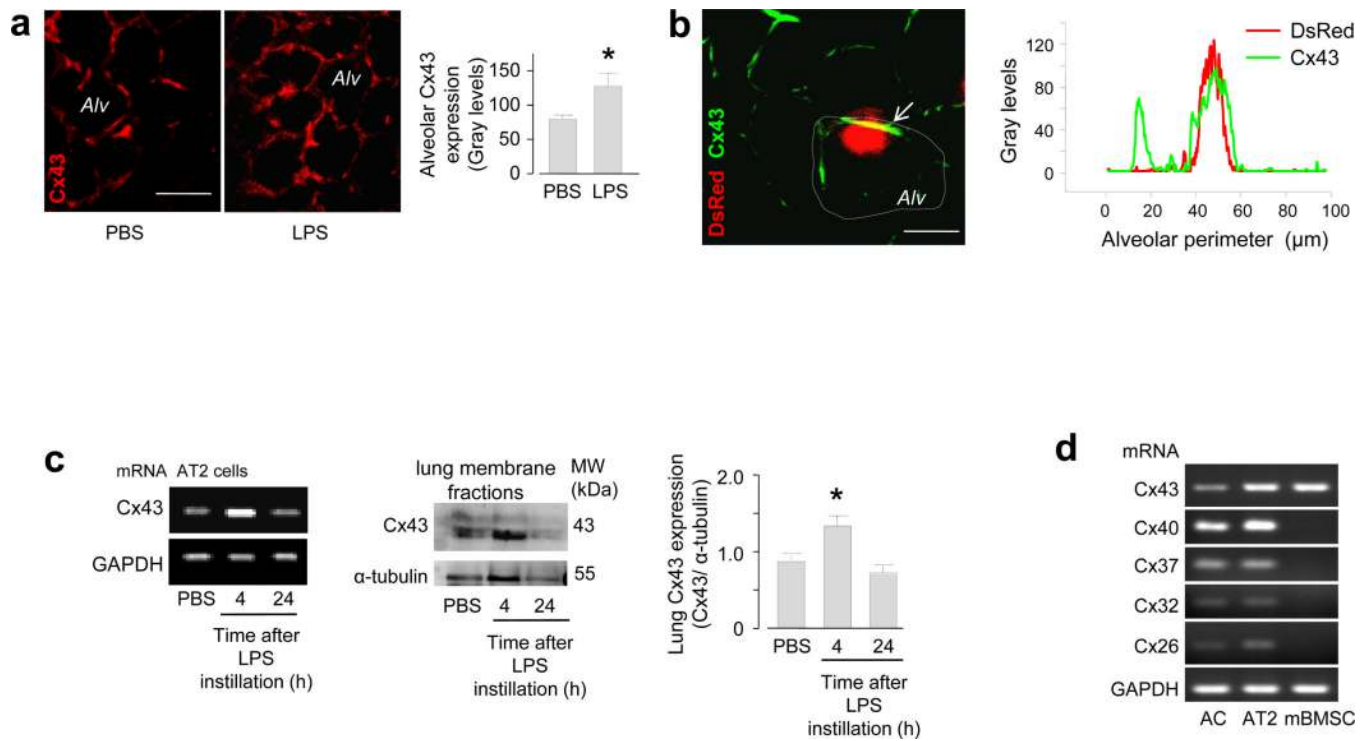
Figure 2. Cx43 expression in mBMSCs and alveoli

(**a**) Images show Cx43 immunofluorescence (*red*) in live alveoli (*Alv*). Group data are for 100 alveoli from 3 lungs in each group. * *p < 0.05* versus PBS. *Line,* 20 μm. (**b**) Image shows a DsRed-expressing mBMSC (*red*) and Cx43 immunofluorescence (*green*) in an alveolus. Tracings are line-scan analyses of the alveolar wall (*dotted line*). The data were replicated four times. *Line,* 10 μm. (**c**) Gels show mRNA (*left*) and protein (*middle*) expressions for Cx43, and densitometry for the immunoblots (*right*). *AT2*, alveolar type 2 cells. *mRNA data replicated three times. n = 4* gels each bar, * *p < 0.05* versus PBS. (**d**) Gels show PCR-amplified DNA sequences for different connexins in primary isolates of alveolar mixed cells (*AC*), AT2 cells and mBMSCs. *Replicated four times.*
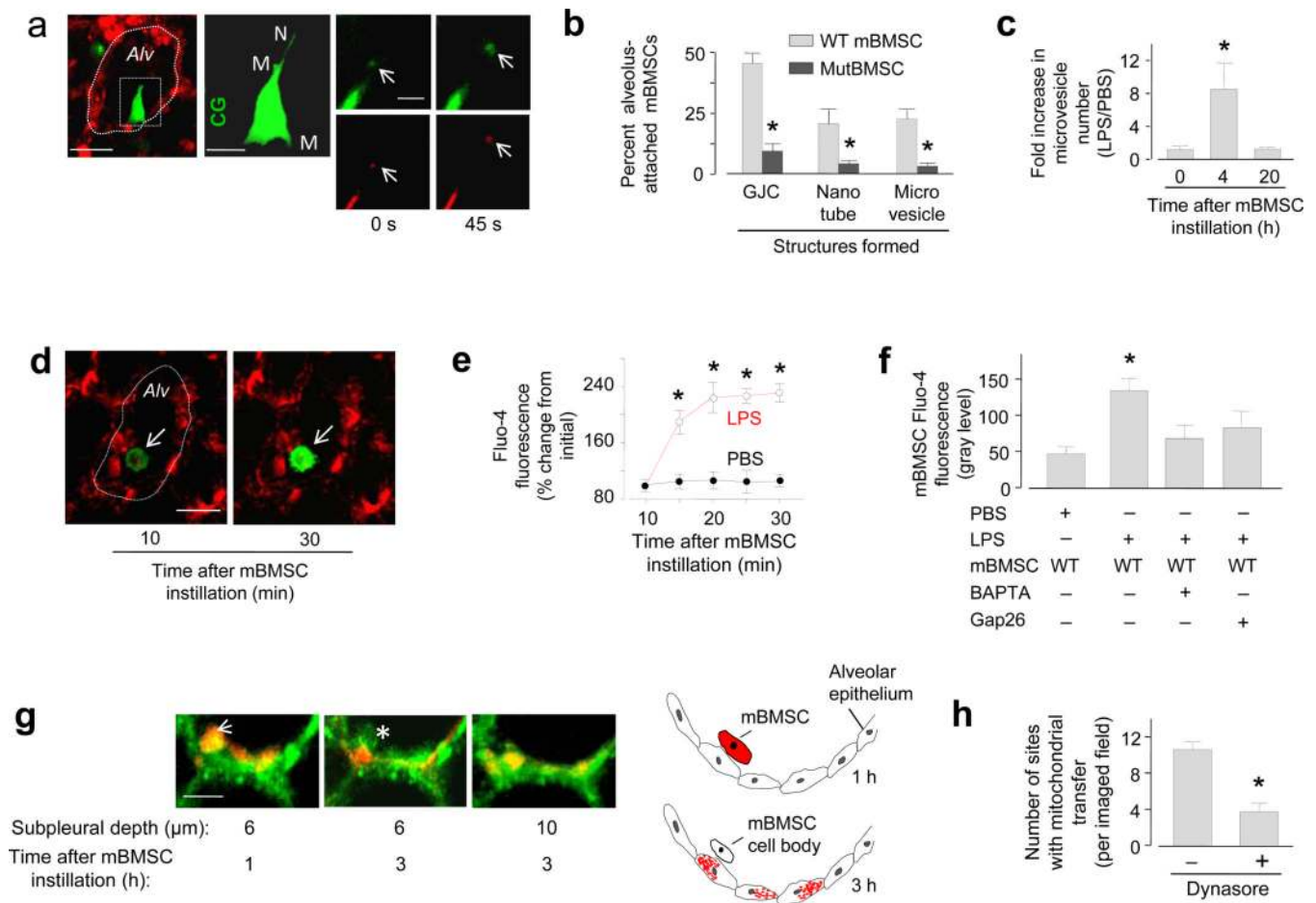
Figure 3. Responses of alveolus-attached mBMSCs 4–8 h after LPS

(**a**) Image of an LPS lung (*left*) shows a mBMSC (*green*) in an alveolus (*red*). Alveolar margins are marked *(dotted line)*. *Line*, 10 μm. High magnification of the selected region (*rectangle*) shows the mBMSC in green rendition in the second panel. *CG,* calcein green. *M,* microvesicles. *N,* nanotube. *Line*, 5 μm. Right panels show a microvesicle (*arrows)* at different time points in green (*calcein green*) and red (*DsRed*) renditions. *Line,* 3 μm. (**b**) Group data for LPS lungs. *n = 40* mBMSCs from 5 lungs in each bar. *mutBMSC,* mBMSCs expressing mutant Cx43. (**c**) Flow cytometry of supernatants derived from homogenates of lungs isolated at the indicated time points after mBMSC instillation. *n = 4* lungs for each bar, * *p < 0.05* versus 0 h. (**d**) Images of an mBMSC (*arrows*) stained with Ca^{2+} dye, fluo-4, in a live alveolus (*red*). *Line,* 10 μm. (**e, f**) Group data are time course of fluo-4 responses in mBMSCs (*e*) and the effects of the indicated treatments (*f*). *n = 9* mBMSCs from 3 lungs for each bar, * *p < 0.05* versus PBS. *WT*, wild-type; *Gap26*, Cx43 inhibiting peptide; *BAPTA-AM,* Ca^{2+} chelator. (**g**) Images show a mBMSC (*arrow*) lying adjacent to the alveolar epithelium (*green*). The cartoon represents the imaging data at two time points. Mitochondria are brown. *Line,* 5 μm. (**h**) Group data for epithelial engulfment. *n = 7* imaged fields from 3 lungs in each bar, * *p < 0.05* versus left bar.

Figure 4. Mitochondrial transfer from BMSCs 24 h after LPS
(**a**) Image of an LPS lung shows AT2 cells (*green*) and instilled mBMSCs *(arrowheads)* expressing DsRed (*red*). *Alv,* alveoli. *Line,* 10 μm. (**b**) Green, red and merged renditions of a single AT2 cell show fluorescence of surfactant protein B (*SPB*) (*upper panel*) and DsRed (*middle panel*). Images were obtained at the indicated levels. The cartoon depicts the optical planes in the AT2 cell. The integrated image projection along the depth (Y-Z) axis, analyzed at the cross-point of the dotted lines in merge image, shows the intracellular location of DsRed fluorescence (*bracket*). *Line,* 2 μm. *Replicated in 5 lungs (20 cells)*. (**c**) Gels show amplified DNA sequences from isolated AT2 cells. *hCO1*, human cytochrome oxidase 1; *hCO2*, human cytochrome oxidase 2; *hBMSC*, human BMSCs; *mBMSC*, mouse BMSCs; *HEK*, human embryonic kidney cells; *mGapdh*: mouse glyceraldehydes 3-phosphate dehydrogenase. *Repeated 4 times*. (**d**) Group data are flow cytometry determinations. *WT*, wild-type mBMSCs; *mutBMSC*, mBMSCs expressing mutant Cx43. $n = 4$ lungs for each bar, * $p < 0.05$ versus 0 h.

Figure 5. Effect of mBMSCs on alveolar bioenergetics
(**a**) Group data are colorimetric determinations in lung homogenates. *WT*, wild-type mBMSCs; *RISP*, Rieske iron-sulfur protein; *siRISP*, mBMSCs treated with siRNA against RISP; *scRISP*, mBMSCs treated with scrambled siRNA; *mut*, mBMSCs expressing a mutant Cx43; *3T3*, mouse 3T3 fibrocytes. $n = 4$ lungs for each bar, * $p < 0.05$ versus PBS. (**b**) Images show immunofluorescence (*upper panel*) and GFP fluorescence (*lower panel*) of the ATP probe, Perceval. *A633*, Alexa fluor 633. *Line,* 20 μm. (**c**) Group data for ATP fluorescence. $n = 3$ imaged field for each bar, * $p < 0.05$ versus PBS. (**d**) Image (*left*) obtained 24 h after LPS, shows alveolar fluorescence of Perceval (*green*) and mBMSC mitochondria (*red, arrows*). *Line,* 20 μm. Magnified images of the selected region (*rectangle in left*) show an alveolus (*Alv*) in green, red and merge renditions. DsRed fluorescence is indicated (*arrowheads*). *Line,* 10 μm. (**e**) Yellow pseudocolor shows changes in alveolar GFP fluorescence (*curved arrows*). We superimposed the red channel rendition of DsRed mitochondria on the alveolar image. The tracings are line-scan analyses. *Line,* 10 μm. (**f**) Group data are changes in Perceval fluorescence. $n = 5$ areas in 3 lungs for each group, * $p < 0.05$ versus LPS alone.
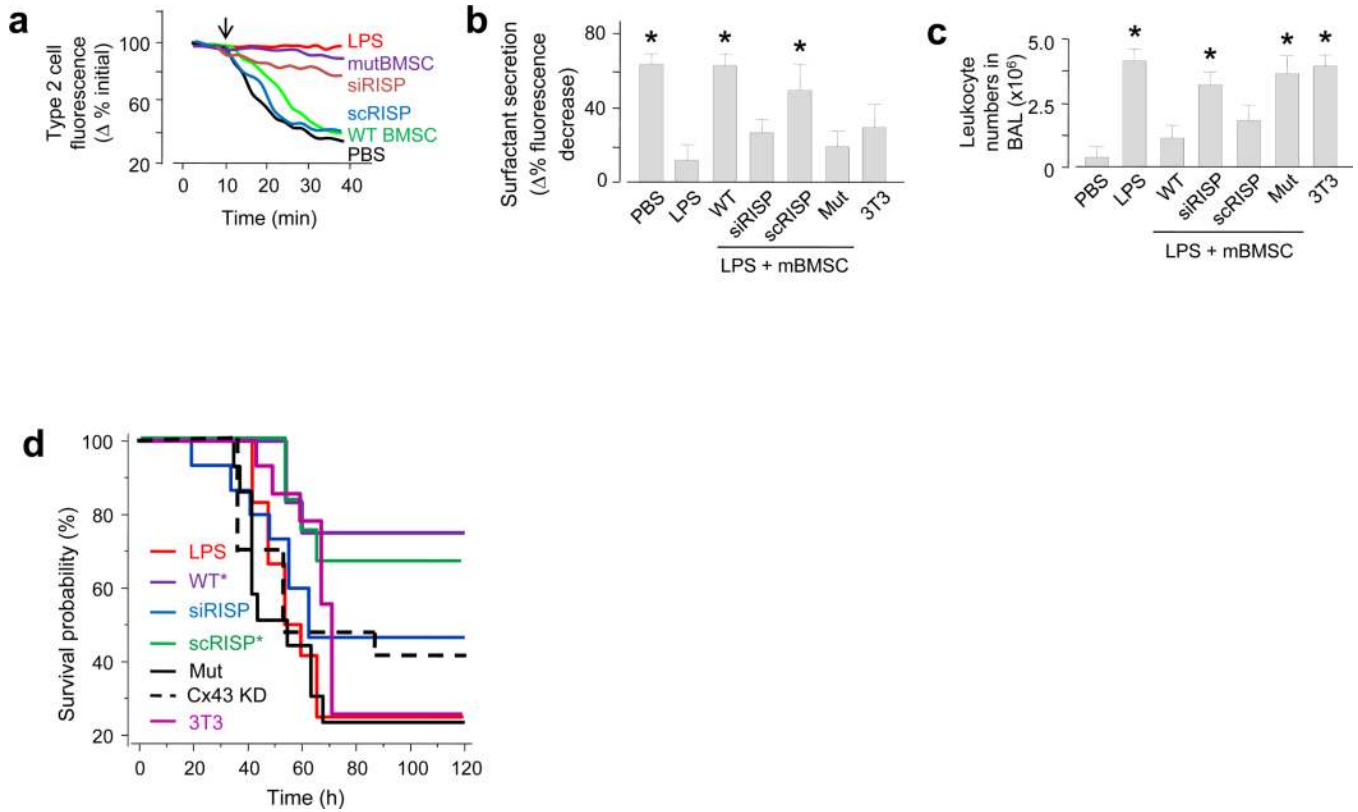
Figure 6. Effect of mBMSCs on injury outcomes
(**a-b**) Inflation (*arrow*)-induced surfactant secretion for single experiments (*a*) and the group (*b*). *WT*, wild type mBMSCs; *siRISP*, mBMSCs containing siRNA against RISP; *scRISP*, mBMSCs containing scrambled siRNA; *mut*, mBMSCs expressing mutant Cx43; *3T3*, mouse 3T3 fibrocytes. *n = 12* cells in 4 lungs for each bar, * *p < 0.05* versus LPS alone. (**c**) Group data for determinations in brochoalveolar lavage (BAL). *n = 4* lungs for each bar, * *p < 0.05* versus PBS. (**d**) Kaplan-Meier plots for mouse survival after instillation of LPS (10 mg kg^{-1}) followed 4 h later by mBMSCs. *Cx43 KD*, mBMSCs treated with siRNA against Cx43. *n = 15* mice for each bar, * *p < 0.05* versus LPS.